

Unresolved spectroscopic binaries with *Gaia* I: Detection & orbital characterization using EDR3 radial velocity errors

DANIEL FOREMAN-MACKEY ¹, QUADRY CHANCE,^{1,2} ANDREW R. CASEY,³ AND
OTHERS TBD

¹*Center for Computational Astrophysics, Flatiron Institute, 162 5th Ave, New York, NY 10010, USA*

²*University of Florida, 211 Bryant Space Science Center, Gainesville, FL 32611, USA*

³*School of Physics & Astronomy, Monash University, Wellington Road, Clayton 3800, Victoria, Australia*

ABSTRACT

The Early Data Release 3 (EDR3) from the *Gaia* Mission includes measurements of the radial velocities (RVs) of more than 7 million targets with the goal of providing a detailed view of the phase space of the Milky Way. Many of these stars are, in fact, members of unresolved multiple star systems and the effects of these orbits are generally seen as a source of contamination in the RV catalog. In this paper, we demonstrate that the published RV error estimates can provide evidence for the existence of an unresolved stellar companion and, under the assumption of a gravitationally-bound binary system, place constraints its orbital parameters. This paper makes three key contributions: (1) We build a flexible data-driven model to estimate *Gaia*’s intrinsic per-transit RV uncertainty as a function of color and apparent magnitude. (2) Using these estimates, we develop a procedure for detecting likely unresolved multiple star systems, and apply this procedure to all targets observed at least 3 times in EDR3. (3) Finally, we derive a physical model for constraining the orbital parameters of a binary system that would be consistent with the observed RV error and number of RV measurements. These parameters are generally only weakly constrained, except for the RV semi-amplitude, which can typically be estimated with a precision of $\sim PPP\%$. To demonstrate the reliability of this method and quantify its completeness, we apply our method to simulated data and catalogs of previously known spectroscopic binaries. We expect that this value-added catalog will be useful for population studies of binary star systems, target selection for precise RV surveys, vetting exoplanet discoveries, and other applications.



Keywords: Astrostatistics (1882) — Binary stars (154) — Radial velocity (1332)

1. INTRODUCTION

By the end of the *Gaia* Mission, it will discover SOME LARGE NUMBER of exoplanet and multiple star systems based on time resolved astrometry and radial velocities of many targets. In the meantime, we only have static measurements of the radial velocity, but it turns out that there is still information in the existing public facing catalog to place constraints on the orbital parameters of multiple systems using the *Gaia* data. It has been previously demonstrated that the published radial velocity and astrometric “errors” can be used a proxy for multiplicity or data quality. In this paper, however, we demonstrate that it is possible to use the reported radial velocity errors and a probabilistic model to place constraints on the radial velocity amplitude and, in some cases, some other properties of the orbit. These measurements are useful for many applications, including (a) discovering black holes, (b) vetting transiting exoplanet discoveries, (c) measuring the masses of a large sample of eclipsing binaries, (d) quantify the binary fraction across the H–R diagram, and (e) informing constraints on exoplanet formation and evolution theory, to name a few.

The fundamental idea of this paper is that even though the *Gaia* catalog only includes a single RV measurement and its error, we can still make calibrated probabilistic inferences about the RV time series. In particular, we know the number of RV observations that were used to measure the RV and its uncertainty. Similarly, we can estimate the expected per-transit RV uncertainty based on the distribution of targets of similar color and magnitude. Using these auxillary values, we can compute the expected distribution of RV error, and compare this to the measured value. It has been previously identified that the RV error measurements scale with RV semi-amplitude (e.g., [Badenes et al. 2018](#), with APOGEE data) (IS THERE A CITATION; add a figure), but below we take this one step further and derive an interpretable, physical, probabilistic model for this effect that allows us to directly infer the semi-amplitude, and weak constraints on the other orbital parameters.

In the following sections, we derive and discuss the components of this model, validate and characterize the performance using simulated data, and compare to archival binary surveys. To start, we build a hierarchical probabilistic model to estimate the per-transit RV measurement uncertainty of the *Gaia* survey as a function of apparent magnitude and observed color.

2. THE BASICS

For each RV target, the *Gaia* EDR3 catalog reports the median RV, an estimate of the error on this median, and the number of individual RV measurements (called “transits”) that were used in this estimate. In our analysis, we ignore the median RV and instead only consider the RV error and number of transits. The RV error ϵ_n for a target n is computed as ([Katz et al. 2019](#))

$$\epsilon_n^2 = \left(\sqrt{\frac{\pi}{2T_n}} s_n \right)^2 + 0.11^2 \quad (1)$$

where

$$s_n^2 = \frac{1}{T_n - 1} \sum_{i=1}^{T_n} (v_{n,i} - \bar{v}_n)^2 \quad (2)$$

is the sample variance of the individual RV measurements $v_{n,t}$. In Equation 2, $t = 1, \dots, T_n$ indexes the T_n transits for target n and

$$\bar{v}_n = \frac{1}{T_n} \sum_{i=1}^{T_n} v_{n,i} \quad (3)$$

is the mean RV. In all that follows, it is much simpler to reason about the sample variance s_n^2 instead of the error on the median ϵ_n , but that isn't a problem because we can compute

$$s_n^2 = \frac{2T_n}{\pi} (\epsilon_n^2 - 0.11^2) \quad (4)$$

for any target, using only values available in the catalog: ϵ_n and T_n .

Now, for a given target n , in the absence of any excess radial velocity signal, and if we know it's per-transit radial velocity measurement uncertainty σ_n , we would expect the quantity

$$\xi_n^2 = \frac{(T_n - 1) s_n^2}{\sigma_n^2} \quad (5)$$

to be chi-squared distributed with $T_n - 1$ degrees of freedom. Based on this argument, we can identify targets that are outliers with respect to this expectation. Figure 1 illustrates this idea using a simulated catalog of *Gaia* RV targets. Here, we generate a sample of *Gaia* RV measurements for binary star systems with orbital parameters drawn from a simple population model, and compare the distribution of measured s_n^2 values to those that we would measure in the absence of binary companions. In Figure 1, both distributions peak near the (known) measurement uncertainty σ^2 —a fact that we will use in the following section to *infer* σ^2 —but the distribution of binary systems shows a tail to larger values of s^2 .

We can even go one step further, and derive the expected sampling distribution for s_n^2 under some model for the excess RV signal. For example, in our case, we want to infer the orbital properties of any binary systems based on the observed s_n^2 . In this case, our model for the expected RV time series is (CITE L&F)

$$\mu_n(t; \theta_n) = v_{0,n} + K_n [\cos(f_n(t) + \omega_n) + e_n \cos \omega_n] \quad , \quad (6)$$

but the following derivation can be used more generally. We can evaluate Equation 6, at observation times $\{t_{n,i}\}_{i=1}^{T_n}$ and orbital parameters $\theta_n = \{K_n, e_n, \omega_n, \dots\}$. Of course, in our case, we don't actually *know* the observation times¹, so we will need

¹ The Gaia Observation Forecast Tool (<https://gaia.esac.esa.int/gost/>) predicts the transit times for astrometric measurements, and we expect the RV measurements will be a subset of these transits, but for most sources that information is not enough to substantially improve our inferences.

to marginalize those out below, but for now, let's proceed as if we do know them. For a given set of parameters, it can be shown (see [Appendix A](#)) that the sampling distribution for our scalar

$$\xi_n^2 = \frac{(T_n - 1) s_n^2}{\sigma_n^2} \quad (7)$$

is a non-central χ^2 distribution with T_n degrees of freedom, and non-centrality parameter

$$\lambda = \sum_{i=1}^{T_n} \left[\frac{\mu_n(t_i; \theta_n) - \bar{\mu}_n}{\sigma_n} \right]^2 \quad (8)$$

where

$$\bar{\mu}_n = \frac{1}{T_n} \sum_{i=1}^{T_n} \mu_n(t_i; \theta_n) \quad (9)$$

is the sample mean of the model evaluated at the observation times. This sampling distribution defines a likelihood function for the parameters θ_n , that we will form the foundation for the probabilistic models built in the following sections.

In all the above, we assumed that the per-observation RV measurement uncertainty σ_n was known. This is not, however, a number that we have access to. Instead, in the next section we derive a hierarchical model for determining a calibrated data-driven estimate of σ_n , as a function of color and apparent magnitude, based on the published EDR3 catalog.

3. ESTIMATING GAIA'S PER-TRANSIT RV MEASUREMENT UNCERTAINTY

A key element of our analysis is that we must be able to make, for each target n in our sample, a reasonably accurate estimate of the per-transit RV measurement uncertainty, called σ_n in the previous section. The *Gaia* catalog does not include this value, but as we will demonstrate, it is possible to make an estimate of σ_n for each target n , using the data available in the catalog. In practice, we will build a data-driven model to infer σ in small bins in observed $G_{\text{BP}} - G_{\text{RP}}$ color and apparent G -band magnitude m_G , making the simplifying assumption that σ is approximately constant at a given color and magnitude. There are other factors, such as distance and stellar evolutionary state, that will affect the measurement uncertainty for a given target, but we find that including these axes has a negligible effect on the inferred σ , and the added complexity is not required for the level of precision required here.

To set up this model, we create a fine grid in color and magnitude, and then for each cell of this grid, we infer σ_n independently of the other bins. In each bin, we assume that all the targets are unresolved binaries with unknown RV semi-amplitude, and we fit for the orbital parameters of each target and the shared RV measurement uncertainty, simultaneously. In principle, we could use the likelihood function defined

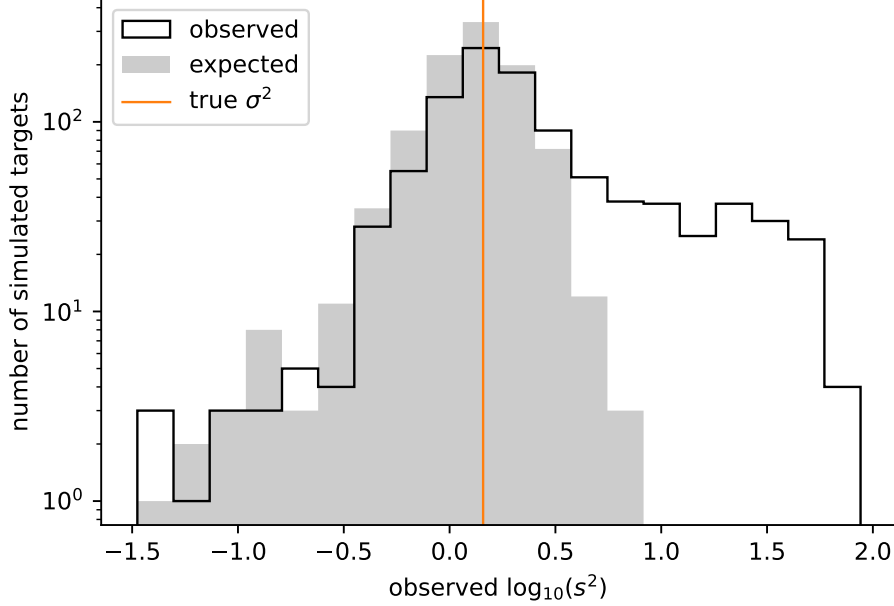



Figure 1. The distribution of RV sample variance s^2 for a simulated population of binary stars observed by *Gaia* (unfilled histogram), compared to the distribution that would have been observed in the absence of companions (shaded histogram). The peak of each distribution is determined by the per-measurement RV uncertainty σ^2 , but the catalog of binaries exhibits a heavy tail to large values of s^2 , which we will use to detect these systems in the real *Gaia* EDR3 catalog. 

in the previous section—and our assumption that the value of σ_n is constant within a small enough color–magnitude bin—to simultaneously infer σ_n , θ_n for a sample of *Gaia* targets. This proposal is made somewhat more complicated by the fact that we also don’t know the observation times $t_{n,i}$ and need to marginalize over them. We discuss this in more detail in SOMESECTION, but here we will make the further simplifying assumptions to define a tractable effective model. We restrict ourselves (for now) to circular orbits and assume that the orbit of each binary is well-sampled. This means that we can approximate the non-centrality parameter as

$$\lambda_{\text{eff},n} = \frac{T_n K_n^2}{2\pi\sigma_n^2} \int_0^{2\pi} \cos^2 \phi \, d\phi = \frac{T_n K_n^2}{2\sigma_n^2}, \quad (10)$$

where K_n is the unknown RV semi-amplitude of the orbit of target n .²

Given this definition for $\lambda_{n,\text{eff}}$, we can define the probabilistic model

$$p(\sigma_n, \{K_n\} | \{T_n, s_n^2\}) \propto p(\sigma_n) \prod_{n=1}^N p(K_n) p(T_n, s_n^2 | \sigma_n, K_n) \quad (11)$$

where the sampling distribution $p(T_n, s_n^2 | \sigma_n, K_n)$ is a non-central χ^2 distribution with $T_n - 1$ degrees of freedom and non-centrality parameter $\lambda_{\text{eff},n}$ defined by [Equa-](#)

² Some intuition for the factor of T_n in [Equation 10](#) can be developed by recognizing that λ is defined in [8](#) as T_n times the sample variance of the model, evaluated at the observed times.

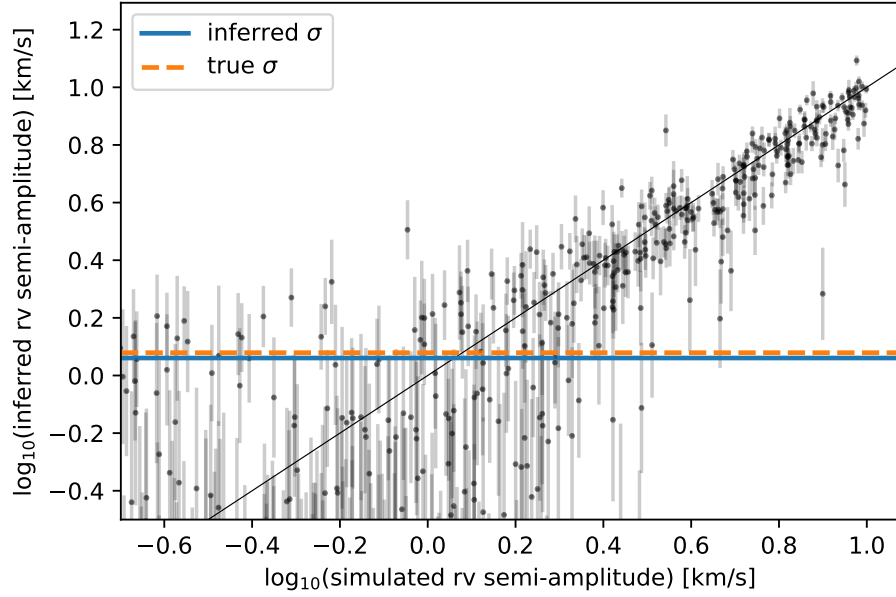


Figure 2. For the simulated *Gaia* catalog from Figure 1, this figure shows the recovered RV semi-amplitude for each simulated target, as a function of its true semi-amplitude. The dashed horizontal line shows the mean RV measurement uncertainty used to simulate the data, compared to the inferred value shown in blue.

tion 10.³ For $p(\sigma_n)$ and $p(K_n)$, we assume the following broad, weakly-informative priors

$$\begin{aligned} \ln \sigma_n &\sim \mathcal{N}(0, 10) \\ \ln K_n &\sim \mathcal{N}(0, 10) \end{aligned} \quad . \quad (12)$$

Given these definitions, we implement this model using the `numpyro` probabilistic programming language and estimate the joint posterior using variational inference. SOME MORE WORDS ABOUT VI.

We validate this procedure by generating a simulated *Gaia* catalog for a sample of unresolved binaries (a large fraction of which have undetectable amplitude) with known orbital parameters and RV measurement uncertainty. This catalog is shown in Figure 1, and Figure 2 demonstrates that this procedure provides an estimate of the true RV uncertainty and, to some extent, the injected RV semi-amplitude for each target. This is not a trivial experiment, because the procedure used to simulate the catalog was not consistent with the simplifying modeling assumptions. In particular, the simulated values for σ_n were generated from a log-normal distribution $\ln \sigma_n \sim \mathcal{N}(\ln \sigma_0, 0.1)$. Furthermore, the simulated RV error values s_n^2 were generated by procedurally sampling observation times and orbital phases, injecting noise, and computing the sample variance. In most cases, the orbits are far from well-sampled.

³ We note that since the sampling distribution is defined for ξ_B^2 , which is a function of σ_n , we must (and do!) include the Jacobian in our definition of $p(T_n, s_n^2 | \sigma_n, K_n)$, with respect to the usual definition of the non-central χ^2 probability density.

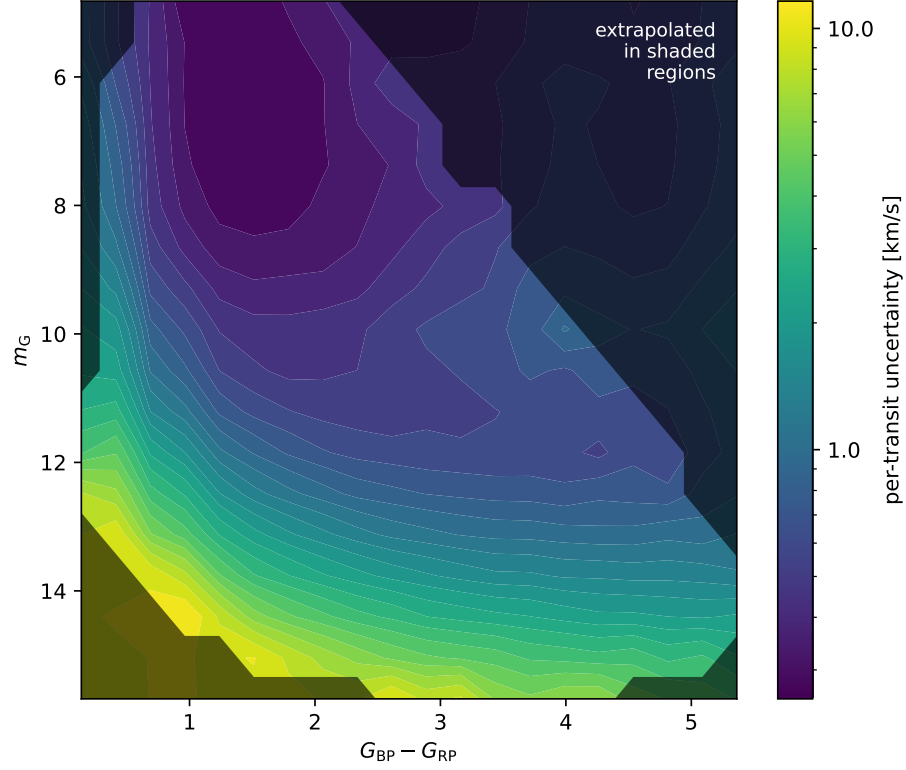


Figure 3. The estimated per-transit *Gaia* RV measurement uncertainty as a function of color and magnitude. The shaded region indicates areas where there were fewer than 50 targets per bin, so this estimate is extrapolated to these regions.



This helps to demonstrate that the accuracy of our inference procedure is not significantly affected by our simplifying assumptions.

In practice, the values for σ_n inferred using the above procedure are somewhat noisy. To regularize our estimates in each bin with more than 1000 targets, we repeat the inference for 5 different, randomly-selected, 1000-target samples, and average the resulting estimates of σ_n . We also perform some light smoothing in color and magnitude to remove some remaining sample noise in bins with few targets. Our final estimate of the per-transit RV uncertainty σ_n as a function of color and magnitude is shown in the color map in Figure 3. The shaded sections of that figure indicate regions where there were fewer than 50 targets per bin. For targets outside the well sampled regime, our estimate of σ_n is extrapolated, and should be considered suspect. Figure 3 shows that the *Gaia* RV spectrograph can reach a precision of better than 300 m s^{-1} for the brightest targets, with more typical values being of order 1 km s^{-1} .

Figure 4 shows the mean RV measurement uncertainty across the color–magnitude diagram, where we have estimated the distance of each source using the inverse parallax. In this figure, there is some shot noise visible around the edges where the target density drops, but there is not otherwise a huge amount of structure. DO WE WANT TO SAY ANYTHING ELSE? ARC: What about the brightest stars (say apparent magnitude less than 6). There are very few stars here, but some people are really

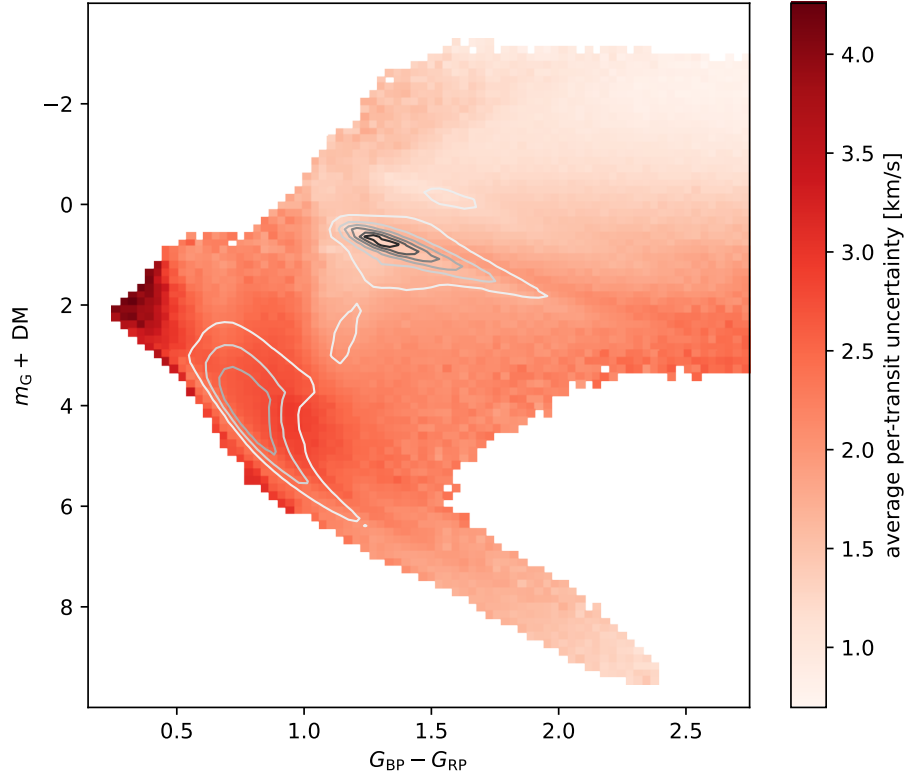


Figure 4. The average per-transit RV uncertainty across the color–magnitude diagram. The contours indicate the density of targets in this same space to guide the eye. Most of the structure in this diagram can be seen near the edges where the number of samples is small. WHAT ABOUT THOSE BLUE BOIS?



interested in these for binarity / young stars / etc. Gaia has some saturating issues at these brightnesses. When combined with the low sample sizes, it makes it pointless to do anything here. Should we mention this?

4. BINARY PROBABILITIES

One side effect of inferring the per-transit radial velocity uncertainty for all sources in *Gaia* is that we also get (for free!) an estimate of the probability that the measured RV error is consistent with what we would expect if the individual RV measurements were Gaussian distributed with this uncertainty. This is some sort of “outlier” probability, but we can use it as a proxy for binarity in the absence of systematic, or other un-accounted for effects. We explore the limitations of such an assumption in the following sections, but it is useful for now to discuss the math for the idealized case here.

As discussed in [section 2](#), if the RV measurements for a given *Gaia* target n includes only Gaussian noise with variance σ_n^2 , the sampling distribution for the measured, normalized RV variance $\xi_n^2 = (T_n - 1) s_n^2 / \sigma_n^2$ is χ^2 with $T_n - 1$ degrees of freedom. Therefore, we can compute the p -value for this null hypothesis as

$$\Pr(\xi^2 > \xi_n^2 \mid \text{null}) = \int_{\xi_n^2}^{\infty} \chi^2(\xi^2; T_n - 1) d\xi^2 \quad . \quad (13)$$

A detailed discussion of the interpretation of p -values is beyond the scope of this paper, but it's useful to recognize that this value quantifies the frequency with which we would expect to mislabel a single star as a binary, given all the assumptions of our model.

We construct a fiducial binary catalog by selecting all targets with a p -value below some threshold P_0 . If our Gaussian model is correct and our estimates of the per-transit measurement uncertainty is accurate, then we would expect targets without companions to pass threshold with probability P_0 . In other words, setting $P_0 = 0.001$, we would expect 1 in 1,000 single targets to pass our cut and be incorrectly labelled as a binary. This number does not directly map to the false positive rate, since that will also depend on the true binary fraction, however, it gives us a tuning parameter that can trade off precision and recall in our selection.

Figure 5 shows the observed distribution of p -values across the full catalog. Our null hypothesis here is that every target is a single star with only Gaussian noise with known variance as estimated in section 3 and, if this hypothesis were correct, we would expect the p -values to be uniformly distributed between zero and one (as indicated by the orange dashed histogram in Figure 5). The fact that the observed distribution is significantly different from this expectation shows that there are a significant number of outliers.

After computing the p -value for every target in our catalog, we can use these values to identify targets that are likely multi-star systems or other kinds of outliers. Figure 6 shows the fraction of targets with $p < 0.001$ as a function of their location in the color-magnitude diagram. In the absence of other sources of noise⁴, this can be interpreted to first order as the binary fraction, but it is important to remember that this is conditioned on the sensitivity of our detection procedure, an effect that we discuss below. With this interpretation, this figure shows some expected structures such as an equal-mass main sequence and an increased binary fraction at higher mass.

5. INFERRING ORBITAL PROPERTIES

As discussed in section 2, we can use these same data to constrain the orbital properties of detected binary systems, under the assumption that there are no significant other dynamical bodies in the system and that the orbit is bound. While we (in principle) constrain all the orbital properties of the system, we find that these data can really only be used to infer the RV semi-amplitude of the orbit. But, as discussed below, for known binary systems, these inferences are reliable and well-calibrated.

In section 2, we derived the non-central χ^2 likelihood function that we combine with the priors discussed below to define the posterior probability density for the orbital parameters conditioned on the measured *Gaia* RV error and the number of RV transits. SOMEFIGURE shows the posterior constraint on the orbital properties of a simulated *Gaia* RV target, compared to the prior density for the same parameters.

⁴ We discuss these other noise sources in SOME SECTION.

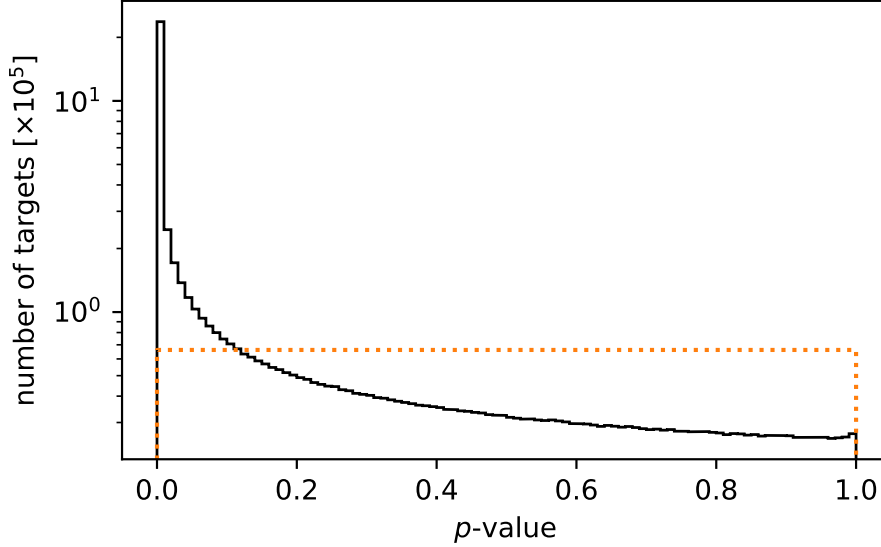


Figure 5. The distribution of p -values across the full sample. In the absence of outliers, we would expect to find the distribution shown as a dashed orange line. ARC: The orange line looks to be at $p \approx 0.7$, but shouldn't we expect it at 1.0?



6. COMPLETENESS & RELIABILITY

In the previous section, we outlined a procedure for identifying possible binary star systems, using the *Gaia* RV errors, but this procedure is not equally sensitive across the full space binary orbital and physical properties. To quantify this effect, we measure the completeness of our survey by simulating a catalog of RV error measurements for a sample of binaries with known properties. Using these simulations, we can estimate the likelihood that our method would detect a binary system as a function of its properties. In particular, the main parameters that determine the detectability of a binary are its RV semi-amplitude of the orbit, per-transit measurement uncertainty, and the number of RV transits.

Figure 7 shows our estimated survey completeness as a function of these primary parameters. This figure mostly shows the expected behavior: our method is more sensitive to systems with larger RV semi-amplitudes that were observed more frequently, with the smallest measurement uncertainty. However, our detection efficiency falls off at larger RV semi-amplitudes, since systems with RV error (ϵ , as defined in Equation 1) larger than 20 km/s are removed from the *Gaia* catalog as outliers, an effect that our simulations include.

We generate a catalog of 100,000 simulated binary systems using the following steps:

1. Sample orbital parameters from the distributions listed in SOMETABLE,
2. Simulate the observation times by randomly sampling T_n times in the range $[0, 668 \text{ d}]$, the approximate duration of *Gaia* DR2, and
3. Calculate the RV signal for a Keplerian orbit observed at the simulated times and return its sample variance.

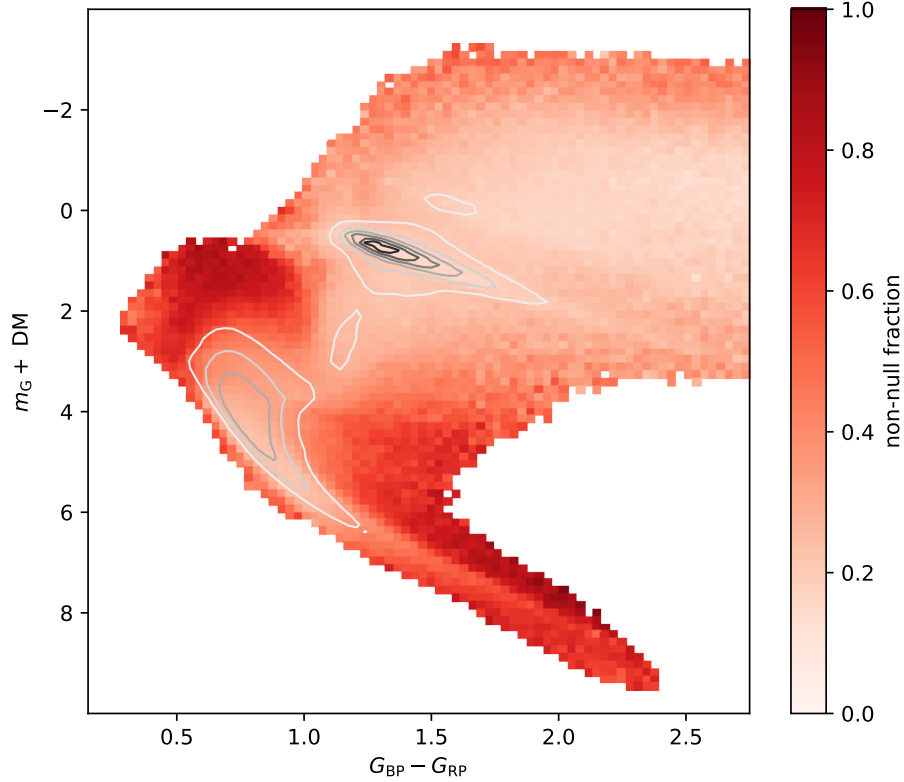


Figure 6. Like Figure 4, but this time the color bar shows the fraction of targets with a p -value less than 0.001. This is an estimate of the fraction of *Gaia* targets that are detectable multiple star systems as a function of color and magnitude. In other words, this can (with the appropriate caveats) be interpreted as the binary fraction across the color–magnitude diagram. Under this interpretation, the equal-mass binary main sequence is clearly visible, and there is an increased binary fraction above the main sequence turn-off, where blue straggler stars are typically observed.



Then for consistency with the *Gaia* processing pipeline, we compute the floored and scaled “error” ϵ (Equation 1) used to construct the official catalog and, like the real catalog, mark any with $\epsilon > 20$ km/s as non-detections. Using this catalog, we evaluate the p -value for each simulated target to determine if it would be detected using our method. We then bin these results as a function of the relevant parameters in Figure 7, in order to estimate the detection efficiency of our method.

Figure 7 doesn’t fully capture all the limitations of this inference. For example, this result assumes that the per-transit RV uncertainty is correctly estimated, and it doesn’t say anything about the false positive rate in our sample.

7. VALIDATION

To validate our methodology, we consider the results of our analysis when applied to targets known to be binary star systems from other spectroscopic surveys. Specifically we compare to (a) the *SB9* (CITE) catalog of spectroscopic binaries collected from the literature, and (b) the sample of binaries detected by the *APOGEE* project (CITE APW). These catalogs have been carefully vetted, and the orbital characterization

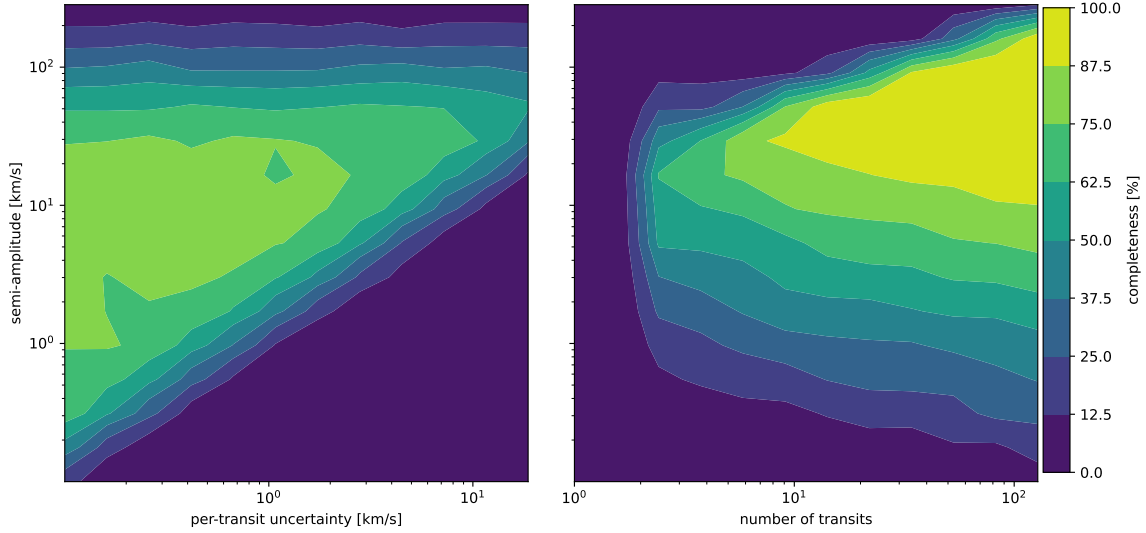


Figure 7. The fraction of simulated binary systems that we recover as a function of its RV semi-amplitude, per-transit RV measurement uncertainty, and the number of RV transits. Unsurprisingly, a larger fraction of these systems are recovered when a target is observed more frequently with smaller measurement uncertainty. Our method is not sensitive to binaries with small semi-amplitudes, since these are indistinguishable from noise, but (perhaps surprisingly) it is also not sensitive to systems with large RV semi-amplitudes since these are likely to be explicitly removed from the catalog because of the large RV error.



was performed using well-sampled RV time series. This means that these systems and their orbital properties are confidently and reliably detected.

7.1. Comparison to the SB9 sample

We cross-matched the *SB9* catalog to *Gaia* EDR3 sources using a HOWBIG angular separation tolerance, and SOME LIMITS on the difference between the *Gaia* G-band magnitude and the *SB9*-reported V-band magnitude. This results in NNN targets in both *SB9* and *Gaia* EDR3’s RV sample. SOMEFIGURE shows the distribution of *p*-values for targets in this cross-match. WHAT DO WE SEE?

The left panel of SOMEOTHERFIGURE shows our measurements of the RV semi-amplitude of each of these targets as a function of the reported *SB9* semi-amplitude. The right panel of the same figure (REF) shows the distribution of normalized residuals, demonstrating that our estimates of the semi-amplitudes are both reliable and well-calibrated.

7.2. Comparison to the APOGEE sample

As with the *SB9* comparison, we cross-match the *APOGEE* targets to the *Gaia* EDR3 RV sample, with THE FOLLOWING DIFFERENCES. We find NNN targets in both catalogs. ONEFIGURE and ANOTHERFIGURE show the same results as FIGURES A AND B ABOVE with similar conclusions. In particular, our measurements of RV semi-amplitude are similarly well-calibrated.

8. DATA ACCESS & CATALOG USAGE

Alongside this paper, we have released an open-access catalog of binary p -values and RV semi-amplitude measurements for all targets in *Gaia* EDR3 with 3 or more RV transits. This catalog, its documentation, and some sample use cases are all available at [SOMEURL](#).

TODO: add some more comments about how one might go about using this catalog for future use cases with reference to Chance et al. (in prep). Also warn about issues with population inference or hierarchical modeling.

9. DISCUSSION

- Potential applications
- Outlook for DR3
- False positive rates

¹ The authors would like to thank the Astronomical Data Group at Flatiron for listening
² to every iteration of this project and for providing great feedback every step of the
³ way.

Facilities: *APOGEE*, *Gaia*

Software: *AstroPy* (Astropy Collaboration et al. 2013, 2018), *JAX* (Bradbury et al. 2018), *NumPy* (Harris et al. 2020), *Matplotlib* (Hunter 2007), *SciPy* (Virtanen et al. 2020)

APPENDIX

A. THE NON-CENTRAL χ^2 DISTRIBUTION

Some fun maths.

REFERENCES

- | | |
|--|---|
| <p>Astropy Collaboration, Robitaille, T. P., Tollerud, E. J., et al. 2013, <i>A&A</i>, 558, A33, doi: 10.1051/0004-6361/201322068</p> <p>Astropy Collaboration, Price-Whelan, A. M., Sipőcz, B. M., et al. 2018, <i>AJ</i>, 156, 123, doi: 10.3847/1538-3881/aabc4f</p> <p>Badenes, C., Mazzola, C., Thompson, T. A., et al. 2018, <i>ApJ</i>, 854, 147, doi: 10.3847/1538-4357/aaa765</p> | <p>Bradbury, J., Frostig, R., Hawkins, P., et al. 2018, <i>JAX: composable transformations of Python+NumPy programs</i>, 0.2.9. http://github.com/google/jax</p> <p>Harris, C. R., Millman, K. J., van der Walt, S. J., et al. 2020, <i>Nature</i>, 585, 357, doi: 10.1038/s41586-020-2649-2</p> |
|--|---|

- Hunter, J. D. 2007, Computing in Science
& Engineering, 9, 90,
doi: [10.1109/MCSE.2007.55](https://doi.org/10.1109/MCSE.2007.55)
- Katz, D., Sartoretti, P., Cropper, M.,
et al. 2019, A&A, 622, A205,
doi: [10.1051/0004-6361/201833273](https://doi.org/10.1051/0004-6361/201833273)
Virtanen, P., Gommers, R., Oliphant,
T. E., et al. 2020, Nature Methods, 17,
261, doi: [10.1038/s41592-019-0686-2](https://doi.org/10.1038/s41592-019-0686-2)